Quantum-based interval selection of the Semi-classical Signal Analysis method

Evangelos Piliouras, Taous-Meriem Laleg-Kirati
Computer Electrical and Mathematical Science and Engineering (CEMSE) division
King Abdullah University of Science and Technology (KAUST)
Thuwal, Kingdom of Saudi Arabia
evangelos.piliouras@kaust.edu.sa, taousmeriem.laleg@kaust.edu.sa

***Abstract*—Semi-classical Signal Analysis (SCSA) is a signal representation algorithm utilizing the Schrödinger eigenvalue problem. The algorithm has found many applications, from signal processing to machine learning and denoising due to its adaptive and localized nature. So far, the algorithm's design parameter was tuned heuristically, without using the knowledge of the quantum mechanical principles residing in the SCSA formulation. In this work, we extend the SCSA framework by calculating the bounds of the reconstruction parameter. The derived bounds are effectively the sampling theorem for SCSA, which is of paramount importance for the application of the theory. Moreover, guidelines towards an optimal choice of the parameter are provided, eliminating the heuristic scanning step.**

***Index Terms*—SCSA, signal decomposition, semi-classical approximation, quantum mechanics, sampling theorem**

I. Introduction

Semi-classical Signal Analysis (SCSA) is a recently proposed decomposition method based on the Schrödinger eigenvalue problem [1], [2]. SCSA possesses very interesting properties like the localization and the adaptivity of the signal components, comparing to the traditional fixed-basis methods like the Fourier transform [3]. The algorithm has found application in filtering [4], [5], and machine learning as a preprocessing tool for feature-related operations [6]. Similar approach is extended to the 2D space, where image reconstruction [7] and denoising [8], [9] are investigated. The method is associated with the adjustability parameter h that is discussed in section II. Since its first statement, more work has been published on the convergence of the algorithm, as $h \to 0$ [10]. While SCSA has gained substantial popularity due to its alternative nature of processing the signal, especially of pulse-shaped nature [5], there has been no defined guidelines on the interval of searching for the optimal value of h, in the sense of the error between the original signal and the decomposed one. In that case, h is swept from large to small values, until minimum error is achieved or a desired number of eigenvalues is reached [4]. Optimization methods were also proposed for the selection of h [11]. The most relevant work was done in [12], where bounds of h are derived as a function of the number of negative eigenvalues and signal characteristics.

This research project has been funded by King Abdullah University of Science and Technology (KAUST) Base Research Fund (BAS/1/1627-01-01)

In this paper, to the best of our knowledge, we present the first work where both the minimum and maximum value of h are derived. As SCSA is heavily based on the Schrödinger eigenvalue problem, the interval is deduced from quantum mechanical principles. This solves the problem of an undefined greedy searching for the optimal value of the representation and provides strong connections between the SCSA and the Fourier transform.

The paper is organized as follows: In section II, the SCSA algorithm is briefly described. In section III, the quantum mechanical concepts that are used for the derivation of the bounds are stated. In section IV, the interval of optimal reconstruction is derived based on known properties of the SCSA algorithm and sampling theory. In sections V and VI, numerical simulations of three signals are realized to assess the validity of the derived bounds, and the results are discussed in the latter section. Moreover, the capability of using the lower bound as a direct decomposition parameter is investigated. In section VII, we conclude our work providing insights on further development of the theory.

II. SCSA Algorithm

The SCSA algorithm aims to decompose a given real non-negative signal y into shape-adapted functions with proper choice of a positive constant h (e.g., minimization of the Mean Squared Error (MSE)). The elements used in the decomposition come from the solution of the Schrödinger eigenvalue problem where the signal plays the role of the potential function:

$$-h^2 \frac{d^2\psi(t)}{dt^2} - y(t)\psi(t) = \lambda\psi(t),\ t \in \mathbb{R}. \tag{1}$$

We are interested in using solely the negative spectrum of (1), with $\lambda = \lambda_{nh}, n = 1 \dots N_h$, where the eigenvalues are discrete and ordered:

$$\lambda_{1h} \leq \lambda_{2h} \cdots \lambda_{N_h h} < 0 \tag{2}$$

The signal is then represented as [1]:

$$y_h(t) = 4h \sum_{n=1}^{N_h} \kappa_{nh} \psi_{nh}^2(t), \tag{3}$$

with:

$$\kappa_{nh}^2 = -\lambda_{nh}, \int_{-\infty}^{+\infty} \psi_{nh}^2(t)dt = 1, n = 1 \dots N_h, \quad (4)$$

where N_h is the number of negative eigenvalues of the problem and ψ_{nh} the associated eigenfunctions. A proper bias precedes the application of the algorithm in case where the signal has negative values. The obtained signal is then shifted back to its correct level. In addition, it is proven [1] that N_h is a decreasing function of h and

$$\lim_{h \to 0} y_h(t) = y(t). \quad (5)$$

The need for well-defined bounds for h arises from the fact that transitioning to the discrete variable, new constraints and phenomena occur. Fundamentally, the limit case described in (5) is not numerically realizable. In parallel, the sampling period T_s in conjunction with h may cause aliasing to the calculated eigenfunctions, which are strongly influenced by the signal itself [13]. Moreover, the number of negative eigenvalues cannot exceed the number of points M of the signal in the case of numerical implementation described in matrix form. Therefore, the definition of these bounds is essential, which can actually reveal the relationship between h and the signal parameters y, T_s, M.

III. Quantum mechanics preliminaries

From (1), it is clear that SCSA is strongly based on quantum mechanics, as the components of decomposition are retrieved from the solution of the Schrödinger eigenvalue problem. The derived bounds of h are based on approximation techniques used extensively in quantum mechanics [14], [15]. The upper bound is based on the perturbation theory, while the lower bound stems from semi-classical approximations. From the numerical solution proposed in [1], we assume a periodic realization of the signal confined in $(-L, L]$. In that case, we have:

$$L = \frac{M}{2} T_s. \quad (6)$$

A. Particle on a circle

When $y(t) = 0$, the system has exact solutions where the periodicity gives rise to the name of the particle on a circle problem [16]. The periodicity condition is expressed as:

$$\psi(t) = \psi(t + 2L), \quad (7)$$

and it is enforced in order to match the solutions of the numerical implementation. The solutions are known as [16]:

$$\psi_{nR}(t) = \frac{1}{\sqrt{2L}} e^{i\frac{(n-1)\pi}{L}t}, \lambda_{nR} = \frac{\pi^2}{L^2} h^2 (n-1)^2, \quad (8)$$

with n being the quantum number arising from the periodicity condition. The subscript R refers to the solutions of the particle on a circle problem. Here $n = 1, \pm 2, \pm 3 \dots$

B. Perturbation theory

The quantum mechanical perturbation theory aims to approximate the effect of a change in the potential of the Schrödinger equation in the eigenvalues and eigenfunctions. The signal $y(t)$ itself is considered as perturbation to the particle on a circle problem, where λ_{nR} are the unperturbed eigenvalues. From [14], the second order perturbation theory of the first eigenvalue ($n = 1$) will aim to approximate the λ_{1h} from (1) as:

$$\lambda_{1h} \approx V_{11} - \sum_{\substack{n=-\infty \\ n \neq 0,1}}^{+\infty} \frac{|V_{1n}|^2}{\lambda_{nR}}, \quad (9)$$

with:

$$V_{1n} = -\int_{-L}^{L} \psi_{1R}^*(t)\, y(t)\, \psi_{nR}(t) dt, \quad (10)$$

where the $*$ denotes complex conjugation. These integrals are effectively the Fourier series coefficients [17] as:

$$V_{1n} = -\frac{1}{2L} \int_{-L}^{L} y(t) e^{i\frac{(n-1)\pi}{L}t} dt = -c_{n-1}^*, \quad (11)$$

The perturbed eigenvalue is written as:

$$\lambda_{1h} \approx -c_0 - \frac{2}{h^2} \left(\frac{L}{\pi}\right)^2 \sum_{n=1}^{+\infty} \frac{|c_n|^2}{n^2}, \quad (12)$$

where the symmetry of the Fourier series was used and the summation index was shifted to start from $n = 1$. In the discrete domain, only the first $\frac{M}{2}$ quantum numbers are addressable ($\pm\frac{M}{2}$), therefore:

$$\lambda_{1h} \approx -c_0 - \frac{2}{h^2} \left(\frac{L}{\pi}\right)^2 \sum_{n=1}^{M/2} \frac{|c_n|^2}{n^2}. \quad (13)$$

C. Quasi-classical eigenfunction approximation

The quasi-classical approximation studies the behavior of the system as $h \to 0$ [15]. This neighborhood of h is exactly the region where SCSA can reconstruct the signal. Therefore it is valid to use such approximation. The eigenvalue problem (1) is expressed as:

$$\frac{d^2\psi(t)}{dt^2} + \frac{y(t) + \lambda}{h^2} \psi(t) = 0. \quad (14)$$

In the semi-classical approximation, the negative spectrum eigenfunctions associated with the eigenvalues λ_{nh} from (1) follow the behavior of [15]:

$$\psi_{nh}(t) \sim e^{\frac{i}{h} \int \sqrt{y(t) - |\lambda_{nh}|} dt}, \quad (15)$$

where an exact solution is retrieved under constant potential. We define:

$$\omega(t) = \frac{1}{h} \frac{d}{dt} \left(\int \sqrt{y(t) - |\lambda_{nh}|} dt \right) = \frac{1}{h} \sqrt{y(t) - |\lambda_{nh}|}, \quad (16)$$

inspired from the concept of instantaneous frequency [18]. From previous work [1], it is known that:

$$-y_{\max} \leq \lambda_{nh} < 0,\ n = 1 \dots N_h. \tag{17}$$

For the regions of t where the approximation holds (as λ_{nh} is a negative quantity), the maximum frequency ω is achieved at $\lambda_{nh} \approx 0$, which yields:

$$\omega_{\max} = \frac{\sqrt{y_{\max}}}{h}. \tag{18}$$

IV. The bounds of h

Proposition 1: Let y be a real valued signal, which we are interested in representing using (3). The values of h yielding accurate representation are restricted in the interval:

$$\frac{T_s}{\pi}\sqrt{y_{\max}} \leq h \leq \frac{T_s}{\pi} M \sqrt{\frac{\sum_{n=1}^{M/2} \frac{|c_n|^2}{2n^2}}{y_{\max} - c_0}}. \tag{19}$$

Proof:

A. Upper bound of h

To approximate the upper bound, it is assumed that the choice of h brings the first eigenvalue to the maximum value of the signal (negated) [1]. As the perturbation theory collapses when the perturbation is large (the smaller the h, the larger the effective y from (1), [14]), the result will yield the smallest of the upper bounds of h. From (13):

$$\lambda_{1h} = -y_{\max} \iff -c_0 - \frac{2}{h_{\max}^2}\left(\frac{L}{\pi}\right)^2 \sum_{n=1}^{M/2} \frac{|c_n|^2}{n^2} = -y_{\max}. \tag{20}$$

Solving for $h_{\max}$ using (6), we obtain:

$$h_{\max} = \frac{T_s}{\pi} M \sqrt{\frac{\sum_{n=1}^{M/2} \frac{|c_n|^2}{2n^2}}{y_{max} - c_0}}. \tag{21}$$

It is remarkable that the derived $h_{\max}$ is shift-invariant, as the Fourier coefficients vanish in a constant value as well as the difference in the denominator removes a signal bias. Intuitively, the upper bound is strongly dependent on the low-frequency components of the signal, as a low-pass filter is implicitly made in the summation term. That kind of behavior indicates noise robustness, as a small amount of noise power is allowed to pass in the $h_{\max}$.

B. Lower bound of h

The derivation of the lower bound is based on the sampling theorem. The reasoning behind the calculation of the maximum frequency was to derive the value of h so that no aliasing is introduced in the eigenfunctions [13]. From (18):

$$\frac{1}{T_s} \geq 2\beta \frac{\omega_{\max}}{2\pi}. \tag{22}$$

Here, $\beta \geq 1$ is the oversampling factor. The lower bound is retrieved as:

$$h_{\min} = \beta \frac{T_s}{\pi}\sqrt{y_{\max}}. \tag{23}$$

The lowest bound is achieved at $\beta = 1$. An interesting relationship of the parameter h and T_s is revealed, as even with large T_s, aliasing seems to be compensated by h. Similar noise robustness is also observed in that case. Analysis of the oversampling factor effect can probably help maximize the lower bound and therefore provide an exact value of h for optimal decomposition.

V. Numerical simulations

For the numerical simulation, the Schrödinger eigenvalue problem is discretized using the spectral method in [1], [19]. The eigenvalue problem (1) is transferred to the discrete domain by using the spectral differentiation for the second derivative with respect to t denoted as T. The signal vector y is transformed to a diagonal matrix Y, where the diagonal elements are the values of the signal at each sample. The eigenvalue problem we solve is:

$$(-h^2 T - Y)\underline{\psi} = \lambda \underline{\psi}, \tag{24}$$

with:

$$T = \left(\frac{\pi}{L}\right)^2 D^{(2)} \tag{25}$$

$$D_{ij}^{(2)} = \begin{cases} -\frac{\pi^2}{3\Delta^2} - \frac{1}{6}, & i = j \\ -\frac{(-1)^k}{2\sin^2(\frac{k\Delta}{2})}, & i \neq j \end{cases}, \Delta = \frac{2\pi}{M}, \tag{26}$$

where $k = i - j$. The calculations refer to an even number of points. A similar matrix D is derived in the odd points case.

Three different signals are tested in this investigation. One sinusoidal signal and a more complex-shaped signal are generated. Moreover, an arterial blood pressure (BP) signal is used as its pulse-shaped nature is suitable for SCSA decomposition [1], [3]. The original signal is downsampled due to its low-frequency character so that all signals have approximately the same number of samples. The error of approximation is defined as:

$$J = T_s ||y - y_h||_2^2. \tag{27}$$

In order to assess the validity of the derived bounds, the interval:

$$h_{\min} \leq h \leq h_{\max}, \tag{28}$$

is scaled, so that we can ensure that the optimal value is free to be found below the derived $h_{\min}$ or above $h_{\max}$. If it is found in between the bounds, then we can conclude that the bounds are accurate. To obtain the proper component expansion, h is varied in the new interval as:

$$\frac{h_{\min}}{10} \leq h \leq 10\, h_{\max}, \tag{29}$$

where this interval is divided in $100M$ points. The optimal h denoted as h_{opt} is defined as the one minimizing J. As an added comparison, the reconstruction using $h_{\min}$ is assessed, to draw conclusions towards an exact value of h eliminating the scanning step.

A. Investigated signals

The generated signals are sampled in the region of:

$$-2\pi \leq t \leq 2\pi, \tag{30}$$

with $M = 164$ points. The functions are:

$$y_1(t) = \cos(t), \tag{31}$$

$$y_2(t) = \frac{1}{\cosh^2(t+\pi)} + tri(t)_{2\pi} + tri(t-\pi)_{\frac{\pi}{2}}, \tag{32}$$

The function tri represents a triangular pulse where the subscript denotes the pulse width.
The BP signal was taken from an extensively used in-silico database [1] [20]. The downsampled signal has the characteristics of:

$$T_s = 8 \cdot 10^{-3} s,\ M = 120 \text{ points}. \tag{33}$$

The BP measurement is in mmHg. The represented signals are given below where the dotted signal represents the approximated one. All signals are reconstructed with high accuracy.

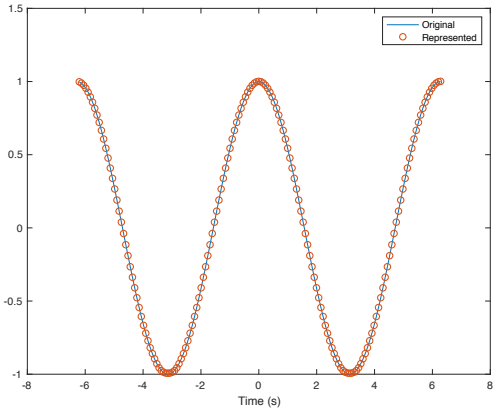

Fig. 1. Cosine signal reconstruction ($N_h = 95$)

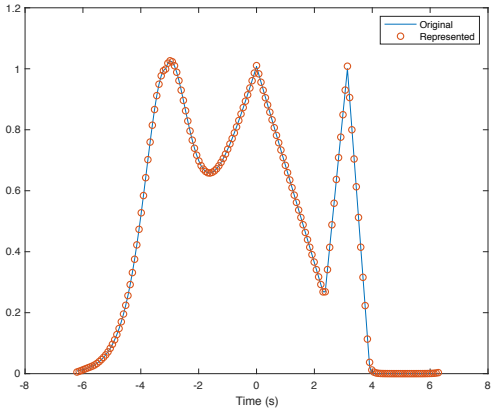

Fig. 2. Complex-shape signal reconstruction ($N_h = 82$)

[1] http://haemod.uk/virtual-database

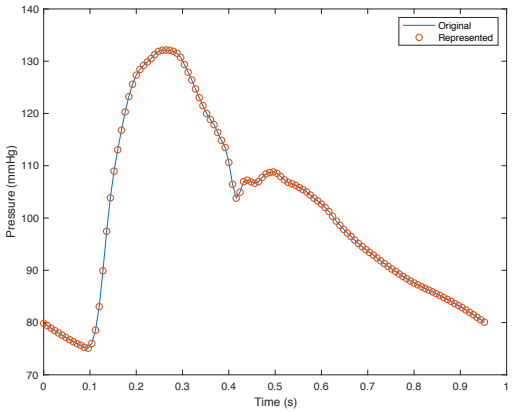

Fig. 3. BP signal reconstruction ($N_h = 53$)

TABLE I
SIGNAL DECOMPOSITION RESULTS

Decomposition data	**Signals**		
	Cosine	***Complex-shape***	***BP signal***
$h_{\min}$	0.0345	0.0247	0.0293
h_{opt}	0.0379	0.0284	0.0573
$h_{\max}$	0.7071	0.8479	0.4081
$J(h_{\text{opt}})$	$0.39 \cdot 10^{-4}$	$0.57 \cdot 10^{-4}$	$0.25 \cdot 10^{-4}$
$J(h_{\min})$	$1.11 \cdot 10^{-4}$	$0.88 \cdot 10^{-4}$	$85.53 \cdot 10^{-4}$
$N_h(h_{\text{opt}})$	95	82	53
$N_h(h_{\min})$	105	94	105

The table contains the bounds of h, the optimal decomposition value h_{opt} and the error between the two signals. Moreover, the number of the negative eigenvalues (signal components) is also provided.

VI. Discussion

From the summary table I, we observe that the optimal value of h is always within the two derived bounds. Moreover, the use of $h_{\min}$ as the exact parameter yields equally good results at the cost of requiring significantly more eigenvalues than in the h_{opt} case. While the existence of the upper bound provides a good starting point for the scanning, the lower bound is of paramount importance as it is illustrated in the figure of the error J as a function of h (Fig. 4) for the BP signal. There is a value of h where the error increases below that value. The minimum h for that case is also marked, to illustrate the validity of the bound. For the sake of completeness, the error as a function of h, for large values of the parameter (Fig. 5) is also provided. In Fig. 5, the error is observed to be an increasing function of h with intermediate local minima. Those dips are attributed to the addition of more eigenvalues as h decreases. It is noteworthy that the percentage difference between $h_{\min}$ and h_{opt} is reflected on the number of negative eigenvalues. This observation was implemented in [4].

VII. Conclusion

In this paper, we provided the first work that aims to define the interval of h where the SCSA algorithm can represent

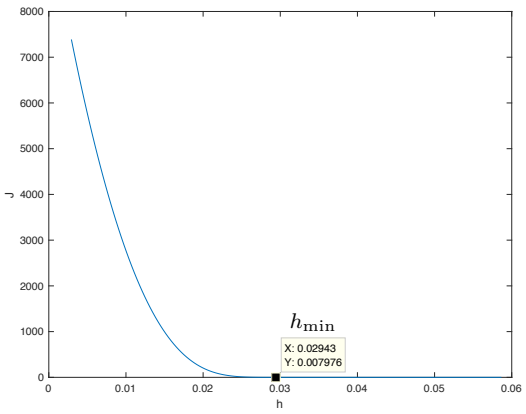

Fig. 4. BP reconstruction error for $\frac{h_{\min}}{10} \leq h \leq h_{opt}$

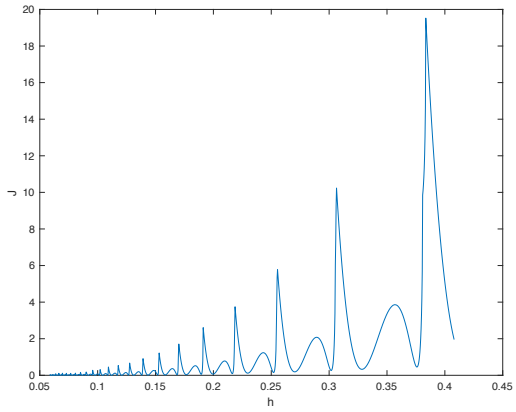

Fig. 5. BP reconstruction error for $h_{opt} \leq h \leq h_{\max}$

a signal optimally, in the sense of (27). The results are effectively the sampling theorem for SCSA, as (19) can be interpreted as the bounds of the sampling rate influenced by the parameter h. A smaller value of h requires a higher sampling rate. Given that as $h \to 0$, we obtain exact representation, we can compare this behavior with the case of a high enough sampling rate when a signal is reconstructed from its samples. Moreover, the methodology used for the derivation of the upper bound can be adapted according to the problem formulation. As discussed, the optimal values for all three signals fall in between the derived bounds. Selecting $h_{\min}$ as the reconstructing value yields equally good results at the cost of the increased number of eigenvalues, paving the way towards a closed-form solution for the selected minimization criteria. For future work, proper choice of the oversampling factor β in (22), as well as higher order perturbation theory, will be investigated. In that sense, the two bounds will start to converge in one unique value of h, where the decomposition of a signal will be immediate. Furthermore, the extension of the bounds to the 2D case will be studied, where the second derivative with respect to time is the Laplacian operator in the image space.

REFERENCES

[1] T. M. Laleg-Kirati, E. Crépeau, and M. Sorine, "Semi-classical signal analysis," *Mathematics of Control, Signals, and Systems*, vol. 25, no. 1, pp. 37–61, 2013. [Online]. Available: https://doi.org/10.1007/s00498-012-0091-1

[2] (2020). [Online]. Available: https://emang-kaust.github.io/index.html

[3] T.-M. Laleg-Kirati, C. Médigue, Y. Papelier, F. Cottin, and A. Van de Louw, "Validation of a Semi-Classical Signal Analysis Method for Stroke Volume Variation Assessment: A Comparison with the PiCCO Technique," *Annals of Biomedical Engineering*, vol. 38, no. 12, pp. 3618–3629, 2010.

[4] A. Chahid, S. Bhaduri, M. Maoui, E. Achten, H. Serrai, and T. Laleg-Kirati, "Residual Water Suppression Using the Squared Eigenfunctions of the Schrödinger Operator," *IEEE Access*, vol. 7, pp. 69 126–69 137, 2019.

[5] P. Li and T. M. Laleg-Kirati, "Signal denoising based on the Schrödinger operator's eigenspectrum and a curvature constraint," aug 2019. [Online]. Available: http://arxiv.org/abs/1908.07758

[6] A. Chahid, T. N. Alotaiby, S. Alshebeili, and T. Laleg-Kirati, "Feature Generation and Dimensionality Reduction using the Discrete Spectrum of the Schrödinger Operator for Epileptic Spikes Detection," in *2019 41st Annual International Conference of the IEEE Engineering in Medicine and Biology Society (EMBC)*, 2019, pp. 2373–2376.

[7] Z. Kaisserli, T.-M. Laleg-Kirati, and A. Lahmar-Benbernou, "A novel algorithm for image representation using discrete spectrum of the Schrödinger operator," *Digital Signal Processing*, vol. 40, pp. 80–87, 2015.

[8] R. Smith, A. Basarab, B. Georgeot, and D. Kouamé, "Adaptive transform via quantum signal processing: application to signal and image denoising," in *2018 25th IEEE International Conference on Image Processing (ICIP)*, 2018, pp. 1523–1527.

[9] A. Chahid, H. Serrai, E. Achten, and T. Laleg-Kirati, "A New ROI-Based performance evaluation method for image denoising using the Squared Eigenfunctions of the Schrödinger Operator," in *2018 40th Annual International Conference of the IEEE Engineering in Medicine and Biology Society (EMBC)*, 2018, pp. 5579–5582.

[10] B. Helffer and T. M. Laleg-Kirati, "On semi-classical questions related to signal analysis," *Asymptotic Analysis*, vol. 75, no. 3-4, pp. 125–144, 2011.

[11] T. M. Laleg-Kirati, J. Zhang, E. Achten, and H. Serrai, "Spectral data de-noising using semi-classical signal analysis: application to localized MRS," *NMR in Biomedicine*, vol. 29, no. 10, pp. 1477–1485, 2016.

[12] D. Y. Liu and T. M. Laleg-Kirati, "Mathematical properties of a semi-classical signal analysis method: Noisy signal case," in *ICSCS 2012 - 2012 1st International Conference on Systems and Computer Science*, 2012, pp. 1–6.

[13] L. Chaparro, "Chapter 8 - sampling theory," in *Signals and Systems Using MATLAB (Second Edition)*, L. Chaparro, Ed. Boston: Academic Press, 2015, pp. 493 – 534. [Online]. Available: http://www.sciencedirect.com/science/article/pii/B9780123948120000085

[14] L. Landau and E. Lifshitz, "Perturbation theory," in *Quantum Mechanics (Third Edition)*. Pergamon, 1977, pp. 133–163. [Online]. Available: http://www.sciencedirect.com/science/article/pii/B978008020940150013X

[15] L. Landau and E. Lifshitz, "The quasi-classical case," in *Quantum Mechanics*. Pergamon, 1977, pp. 164–196. [Online]. Available: http://www.sciencedirect.com/science/article/pii/B9780080209401500141

[16] B. Zwiebach. (2020) Quantum Physics I. [Online]. Available: https://ocw.mit.edu/courses/physics/8-04-quantum-physics-i-spring-2016

[17] L. Chaparro, "Chapter 4 - frequency analysis: The Fourier series," in *Signals and Systems Using MATLAB (Second Edition)*, L. Chaparro, Ed. Boston: Academic Press, 2015, pp. 263 – 332. [Online]. Available: http://www.sciencedirect.com/science/article/pii/B9780123948120000048

[18] B. Boashash, "Estimating and interpreting the instantaneous frequency of a signal. I. Fundamentals," *Proceedings of the IEEE*, vol. 80, no. 4, pp. 520–538, 1992.

[19] L. N. Trefethen, *Spectral Methods in MATLAB*, 2000. [Online]. Available: https://epubs.siam.org/doi/abs/10.1137/1.9780898719598

[20] M. Willemet, P. Chowienczyk, and J. Alastruey, "A database of virtual healthy subjects to assess the accuracy of foot-to-foot pulse wave velocities for estimation of aortic stiffness," *American Journal of Physiology-Heart and Circulatory Physiology*, vol. 309, no. 4, pp. H663–H675, 2015.